4. D. Jiang *et al.*, *Nat. Commun.* **5**, 5708 (2014).
5. S. Qin, J. Kim, Q. Niu, C. K. Shih, *Science* **324**, 1314–1317 (2009).
6. Q. Y. Wang *et al.*, *Chin. Phys. Lett.* **29**, 037402 (2012).
7. C. Xu *et al.*, *Nat. Mater.* **2015**, 10.1038/nmat4374 (2015).
8. A. M. Goldman, *Int. J. Mod. Phys. B* **24**, 4081–4101 (2010).
9. M. P. A. Fisher, *Phys. Rev. Lett.* **65**, 923–926 (1990).
10. D. Ephron, A. Yazdani, A. Kapitulnik, M. R. Beasley, *Phys. Rev. Lett.* **76**, 1529–1532 (1996).
11. Y. Lee *et al.*, *Phys. Rev. Lett.* **106**, 136809 (2011).
12. P. Gallagher, M. Lee, J. R. Williams, D. Goldhaber-Gordon, *Nat. Phys.* **10**, 748–752 (2014).
13. K. Ueno *et al.*, *Nat. Nanotechnol.* **6**, 408–412 (2011).
14. J. T. Ye *et al.*, *Nat. Mater.* **9**, 125–128 (2010).
15. J. T. Ye *et al.*, *Science* **338**, 1193–1196 (2012).
16. S. Jo, D. Costanzo, H. Berger, A. F. Morpurgo, *Nano Lett.* **15**, 1197–1202 (2015).
17. W. Shi *et al.*, *Sci. Rep.* **5**, 12534 (2015).
18. S. G. Haupt, D. R. Riley, J. T. McDevitt, *Adv. Mater.* **5**, 755–758 (1993).
19. S. G. Haupt *et al.*, *Proc. SPIE* **2158**, 238–249 (1994).
20. A. T. Bollinger *et al.*, *Nature* **472**, 458–460 (2011).
21. X. Leng, J. Garcia-Barriocanal, S. Bose, Y. Lee, A. M. Goldman, *Phys. Rev. Lett.* **107**, 027001 (2011).
22. S. W. Zeng *et al.*, *Phys. Rev. B* **92**, 020503 (2015).
23. S. Shamoto *et al.*, *Physica C* **306**, 7–14 (1998).
24. X. Chen, L. Zhu, S. Yamanaka, *J. Solid State Chem.* **169**, 149–154 (2002).
25. S. Yamanaka, H. Kawaji, K. Hotehama, M. Ohashi, *Adv. Mater.* **8**, 771–774 (1996).
26. T. Ito *et al.*, *Phys. Rev. B* **69**, 134522 (2004).
27. T. Takano, A. Kitora, Y. Taguchi, Y. Iwasa, *Phys. Rev. B* **77**, 104518 (2008).
28. Y. Taguchi, A. Kitora, Y. Iwasa, *Phys. Rev. Lett.* **97**, 107001 (2006).
29. See the supplementary materials on *Science* Online.
30. B. I. Halperin, D. R. Nelson, *J. Low Temp.* **36**, 599–616 (1979).
31. Y.-H. Lin, J. Nelson, A. M. Goldman, *Phys. Rev. Lett.* **109**, 017002 (2012).
32. L. G. Aslamazov, A. I. Larkin, *Phys. Lett.* **26A**, 238–239 (1968).
33. K. Maki, *Prog. Theor. Phys.* **39**, 897–906 (1968).
34. R. S. Thompson, *Phys. Rev. B* **1**, 327–333 (1970).
35. M. Tinkham, *Introduction to Superconductivity* (Dover, New York, ed. 2, 2004).
36. K. Ueno *et al.*, *Phys. Rev. B* **89**, 020508 (2014).
37. T. Brumme, M. Calandra, F. Mauri, *Phys. Rev. B* **89**, 245406 (2014).
38. T. Takano *et al.*, *J. Phys. Soc. Jpn.* **80**, 023702 (2011).
39. M. V. Feigel'man, V. B. Geshkenbein, A. I. Larkin, *Physica C* **167**, 177–187 (1990).
40. Y. Qin, C. L. Vicente, J. Yoon, *Phys. Rev. B* **73**, 100505 (2006).
41. E. Shimshoni, A. Auerbach, A. Kapitulnik, *Phys. Rev. Lett.* **80**, 3352–3355 (1998).
42. T. Schneider, S. Weyeneth, *Phys. Rev. B* **90**, 064501 (2014).
43. N. Mason, A. Kapitulnik, *Phys. Rev. Lett.* **82**, 5341–5344 (1999).

ACKNOWLEDGMENTS

We thank M. Nakano and Y. Nakagawa for technical support, M. Yoshida for fruitful discussions, and N. Shiba for useful comments on the manuscript. Y.S. was supported by the Japan Society for the Promotion of Science (JSPS) through a research fellowship for young scientists. J.T.Y. acknowledges the funding from the European Research Council (consolidator grant no. 648855 lg-QPD). This work was supported by the Strategic International Collaborative Research Program (SICORP-LEMSUPER) of the Japan Science and Technology Agency, Grant-in-Aid for Specially Promoted Research (no. 25000003) from JSPS and Grant-in Aid for Scientific Research on Innovative Areas (no. 22103004) from MEXT of Japan.

SUPPLEMENTARY MATERIALS

www.sciencemag.org/content/350/6259/409/suppl/DC1
Materials and Methods
Supplementary Text
Figs. S1 to S6
References (*44*–*49*)

31 July 2014; accepted 15 September 2015
Published online 1 October 2015
10.1126/science.1259440

TOPOLOGICAL MATTER

Evidence for the chiral anomaly in the Dirac semimetal Na_3Bi

Jun Xiong,[1] Satya K. Kushwaha,[2] Tian Liang,[1] Jason W. Krizan,[2] Max Hirschberger,[1] Wudi Wang,[1] R. J. Cava,[2] N. P. Ong[1]*

In a Dirac semimetal, each Dirac node is resolved into two Weyl nodes with opposite "handedness" or chirality. The two chiral populations do not mix. However, in parallel electric and magnetic fields (E||B), charge is predicted to flow between the Weyl nodes, leading to negative magnetoresistance. This "axial" current is the chiral (Adler-Bell-Jackiw) anomaly investigated in quantum field theory. We report the observation of a large, negative longitudinal magnetoresistance in the Dirac semimetal Na_3Bi. The negative magnetoresistance is acutely sensitive to deviations of the direction of B from E and is incompatible with conventional transport. By rotating E (as well as B), we show that it is consistent with the prediction of the chiral anomaly.

The notion of handedness, or chirality, is ubiquitous in the sciences. A fundamental example occurs in quantum field theory. Massless fermions segregate into left- or right-handed groups (they spin clockwise or anticlockwise, respectively, if viewed head on). Because the two groups never mix, we say that chirality is conserved. However, mixing occurs once electromagnetic fields are switched on. This induced breaking of chiral symmetry, known as the chiral anomaly (*1*), was first studied in pion physics, where it causes neutral pions to decay faster than charged pions by a factor of 3×10^8 (*1*–*3*). In 1983, it was proposed that the anomaly may be observed in a crystal (*4*). This goal now seems attainable (*5*–*11*) in the nascent field of Dirac/Weyl semimetals (*12*–*15*).

In Na_3Bi (*14*), strong spin-orbit coupling inverts the bands derived from the Na-3s and Bi-6p orbitals, forcing them to cross at the wave vectors $\mathbf{K}_\pm = (0, 0, \pm k_D)$, with $k_D \sim 0.1$ Å^{-1} (*16*, *17*). Because symmetry constraints forbid hybridization (*13*, *15*), we have topologically protected Dirac states with energy $E(\mathbf{k}) = \hbar v|\mathbf{k}|$, where the wave vector $\mathbf{k}$ is measured from $\mathbf{K}_\pm$ and v is the Fermi velocity (Fig. 1A). Furthermore, symmetry dictates that each Dirac node resolves into two massless Weyl nodes with chiralities $\chi = \pm 1$ that preclude mixing [we calculate χ in (*18*)]. As discussed in (*4*), parallel electric and magnetic fields $\mathbf{E}||\mathbf{B}$ should cause charge pumping between the Weyl nodes, observable as a negative longitudinal magnetoresistance (LMR) (*6*–*11*).

Inspired by these ideas, experimental groups have recently reported negative LMR in $Bi_{1-x}Sb_x$ (*19*), Cd_3As_2 (*20*, *21*), $ZrTe_5$ (*22*), and TaAs (*23*). However, because negative LMR also exists in semimetals that do not have a Dirac dispersion [e.g., $Cd_xHg_{1-x}Te$ (*24*) and $PdCoO_2$ (*25*)], it is desirable to go beyond this observation. Here, we found that in Na_3Bi the enhanced current is locked to the **B** vector and hence can be steered by rotating **B**, even for weak fields.

Crystals of Na_3Bi grow as millimeter-sized, deep purple, hexagonal plates with the largest face parallel to the *a*-*b* plane (*26*). We annealed the crystals for 10 weeks before opening the growth tube. Crystals were contacted using silver epoxy in an argon glovebox to avoid oxidation, and were then immersed in paratone in a capsule before rapid cooling. Initial experiments in our lab (*27*) on samples with a large Fermi energy E_F (400 mV) showed only a positive magnetoresistance (MR) with the anomalous *B*-linear profile reported in Cd_3As_2 (*20*).

Progress in lowering E_F in Na_3Bi has resulted in samples that display a nonmetallic resistivity ρ versus T profile, a low Hall density $n_H \sim 1 \times 10^{17}$ cm^{-3} (Fig. 1C), and a notably large, negative LMR (Fig. 1D). We explain why the negative LMR is not from localization in (*18*). We estimate the Fermi wave vector $k_F = 0.013$ Å^{-1} (smaller than k_D by a factor of 8). Below ~10 K, the conductivity is dominated by conduction band carriers with mobility $\mu \sim 2600$ cm^2 V^{-1} s^{-1}. Because the energy gap is zero, holes in the valence band are copiously excited even at low T. Above 10 K, the increased hole population leads to a steep decrease in ρ and an inversion of the sign of R_H at 62 K. From the maximum in R_H at 105 K, we estimate that $E_F \sim 3k_BT \sim 30$ mV. These numbers are confirmed by Shubnikov–de Haas (SdH) oscillations observed in the resistivity matrix element ρ_{xx} when **B** is tilted toward **c** (Fig. 2A). The index plot of $1/B_n$ (Fig. 2B), where B_n locates the SdH extrema, yields a Fermi surface (FS) cross section $S_F = 4.8 \pm 0.3$ T, which gives $E_F = 29 \pm 2$ mV, in good agreement with R_H. The density inferred from S_F ($n_e = 1.4 \times 10^{17}$ cm^{-3}) is slightly higher than n_H. The deviation from the straight line in Fig. 2B is consistent with a (spin gyromagnetic) g factor of ~20, whereas $g \approx 40$ has been estimated for Cd_3As_2 (*28*). The SdH oscillations imply that E_F enters the $N = 0$ Landau level at $B = 6$ to 8 T.

[1]Department of Physics, Princeton University, Princeton, NJ 08544, USA. [2]Department of Chemistry, Princeton University, Princeton, NJ 08544, USA.
*Corresponding author. E-mail: npo@princeton.edu

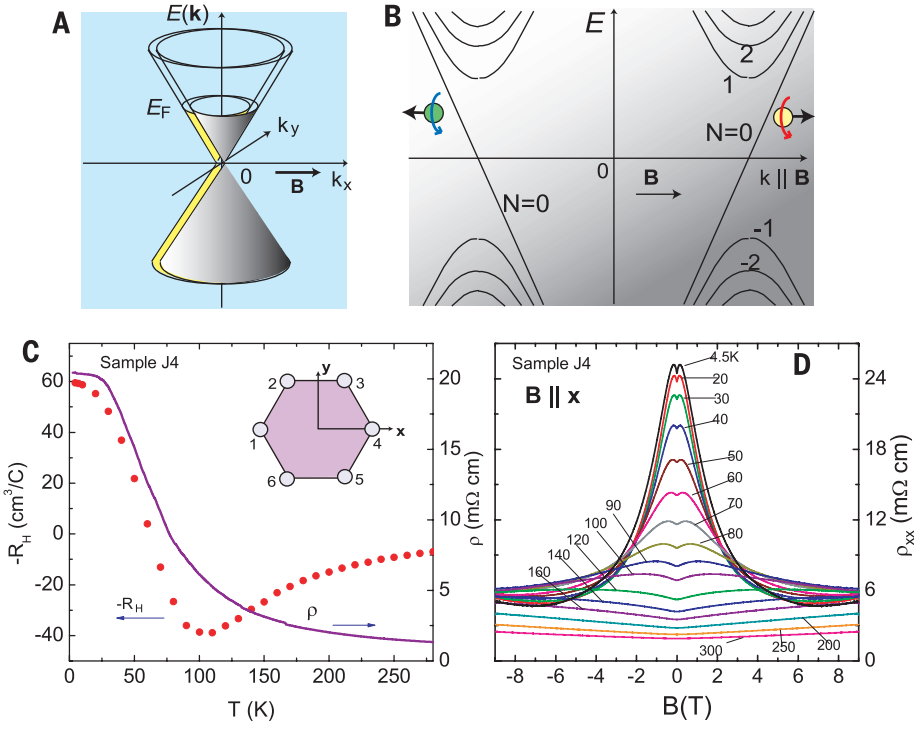

Fig. 1. Weyl nodes and negative longitudinal magnetoresistance in Na_3Bi. (**A**) Sketch of a Dirac cone centered at K_+ represented as two massless Weyl nodes (slightly displaced) with distinct chiralities $\chi = -1$ (gray cone) and +1 (yellow). (**B**) An intense B field widens the node separation due to the spin Zeeman energy (separation exaggerated for clarity). The Weyl states are quantized into LLs. The $N = 0$ LL has a linear dispersion with slopes determined by χ. The yellow and green balls represent χ. An E-field ||**B** generates an axial current observed as a large, negative LMR. (**C**) The T dependence of the resistivity ρ in $B = 0$, as inferred from $R_{14,23}$ (I applied to contacts 1 and 4, voltage measured across contacts 2 and 3) and the Hall coefficient R_H (inferred from $R_{14,35}$). Inset shows the hexagonal crystal J4 (1 mm on each side and 0.5 mm thick), contact labels, and the x and y axes. R_H is measured in $B < 2$ T applied ||**c**. At 3 K, R_H corresponds to a density $n = 1.04 \times 10^{17}$ cm^{-3}. The excitation of holes in the valence band leads to a sign change in R_H near 70 K and a steep decrease in ρ. (**D**) Longitudinal magnetoresistance $\rho_{xx}(B, T)$ at selected T from 4.5 to 300 K measured with **B**||$\hat{\mathbf{x}}$ and I applied to contacts 1 and 4. The steep decrease in $\rho_{xx}(B, T)$ with increasing B at 4.5 K reflects the onset of the axial current in the lowest LL. As T increases, occupation of higher LLs in conduction and valence bands overwhelms the axial current.

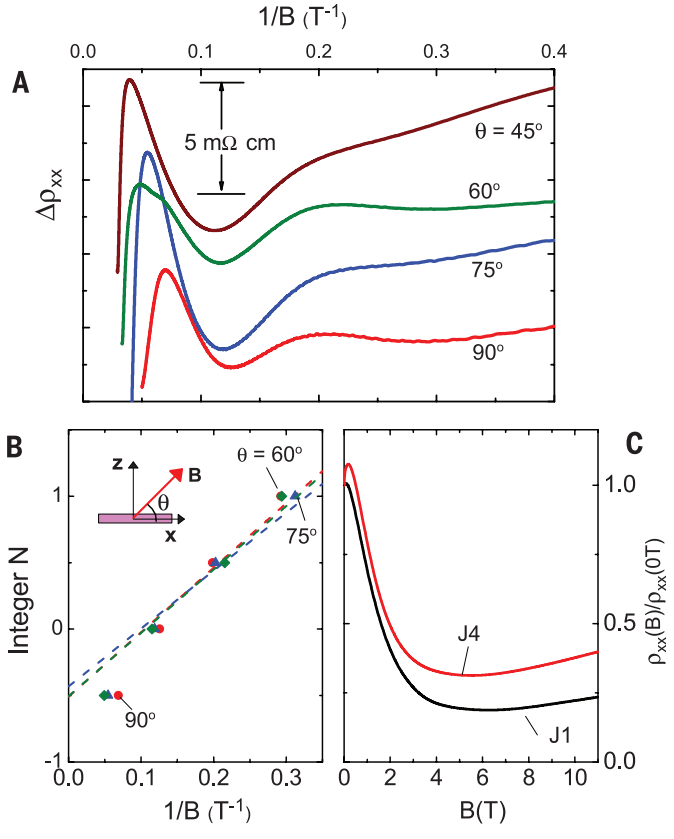

Fig. 2. Shubnikov–de Haas oscillations in Na_3Bi. (**A**) SdH oscillations resolved in ρ_{xx} for several tilt angles θ (relative to $\hat{\mathbf{x}}$) after subtraction of the positive B-linear MR background (vertical scale as shown). The subtraction is explained in (*18*). (**B**) Landau level index N versus $1/B_n$, where B_n locates the extrema of the oscillations at selected θ (θ is defined in the inset). Uncertainties in $1/B_n$ are less than 10% (*18*). The slope at small B yields $S_F = 4.8 \pm 0.3$ T, $k_F = 0.013$ Å^{-1}, and $E_F = 29 \pm 2$ mV. The deviation at large B is consistent with a g^* value of ~20 (*18*). (**C**) Field profiles of ρ_{xx} (inferred from $R_{14,23}$) in samples J1 and J4, with **B**||**I**. The $N = 0$ LL is entered at $B = 6$ to 8 T. The slight increase for $B > 5$ T reflects the narrow width of the axial current. A slight misalignment of B (the uncertainty here is ±1°) allows the B-linear positive MR component to appear as a background at large B.

The Landau levels (LLs) of the Weyl states in a strong **B** are sketched in Fig. 1B. In addition to the LLs, the spin Zeeman energy shifts the nodes away from $\mathbf{K}_+$ by $\delta k_N = \chi g^* \mu_B B/(\hbar v)$, where $\hbar$ is the Planck constant divided by 2π and μ_B is the Bohr magneton (*14*, *18*). For clarity, we show the shifts exaggerated. A distinguishing feature of Weyl states is that the lowest LL ($N = 0$) disperses linearly to the right or left depending on χ. Application of **E**||**B** leads to a charge pumping rate between the two branches

$$W = \chi \frac{e^3}{4\pi^2\hbar^2} \mathbf{E} \cdot \mathbf{B} \qquad (1)$$

This is the chiral anomaly (*4*–*11*). The longitudinal (axial) current relaxes at a rate $1/\tau_a \sim |M|^2 eB/\hbar w$, where M is the matrix element for impurity scattering and $eB/\hbar v$ is the LL degeneracy (*8*). Hence, the chiral conductivity $\sigma_\chi \sim W\tau_a$ is independent of B in the quantum limit. Equation 1 and the expression for $1/\tau_a$ apply in the quantum limit at high fields (when only the lowest LL is occupied). However, we emphasize that even in weak fields when many LLs are occupied, the axial current remains observable. In the weak-B limit, Son and Spivak (*9*) showed that

$$\sigma_\chi = \frac{e^2}{4\pi^2\hbar c} \frac{v}{c} \frac{(eBv)^2}{E_F^2} \tau_a \qquad (2)$$

with $1/\tau_a$ now independent of B. As B increases, σ_χ grows as B^2 [see also (*29*)] but saturates to a B-independent value in the quantum limit.

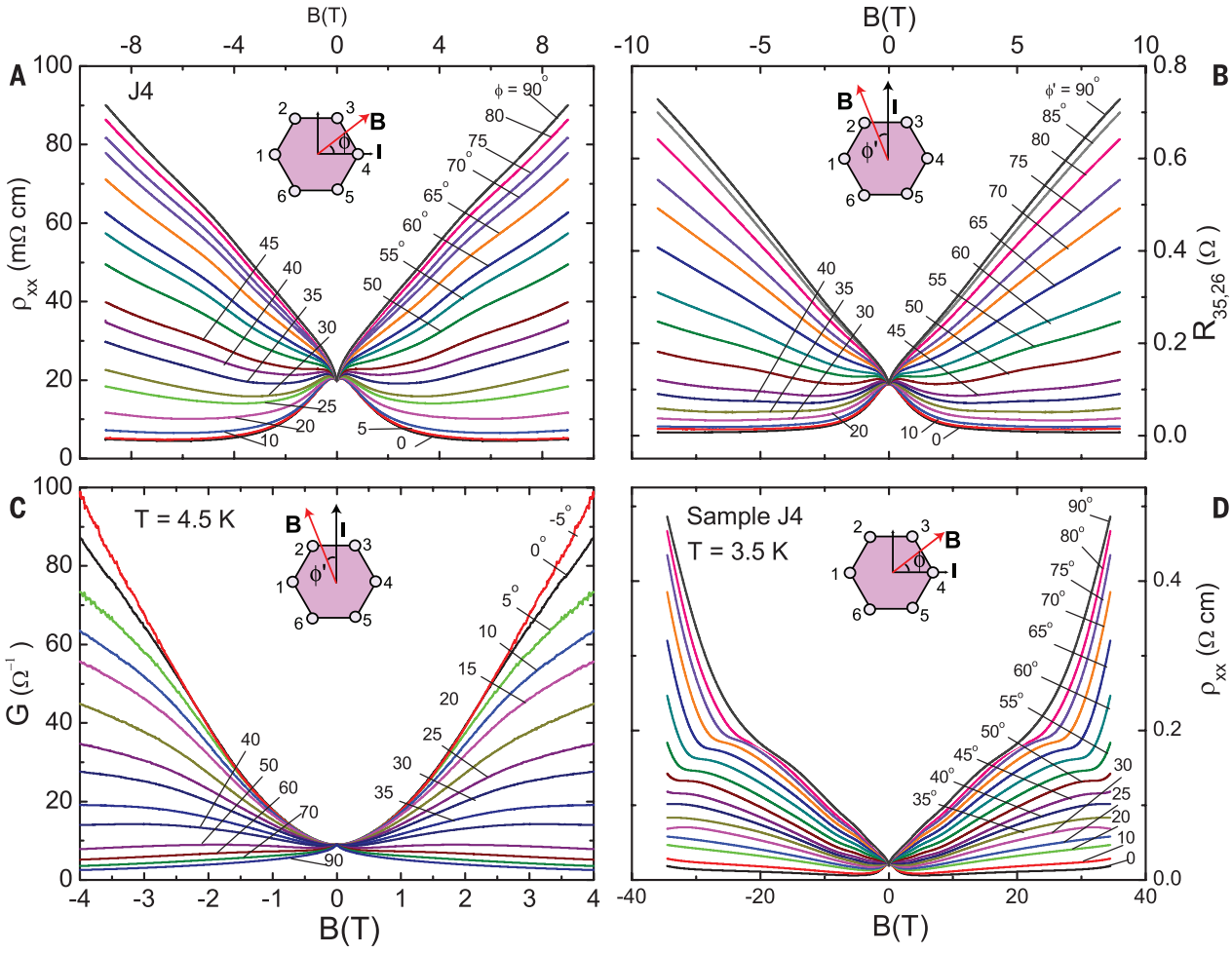

Fig. 3. Evidence for axial current in Na_3Bi. Transport measurements were taken on sample J4 in an in-plane field **B**. (**A**) Resistivity ρ_{xx} versus B at selected field-tilt angles ϕ to the x axis (inferred from resistance $R_{14,23}$; see inset). For $\phi = 90°$, ρ_{xx} displays a B-linear positive MR. However, as $\phi \to 0°$ (**B**$||\hat{\mathbf{x}}$), ρ_{xx} is strongly suppressed. (**B**) $R_{35,26}$ with **E** rotated by 90° relative to (A) (**B** makes an angle ϕ' relative to $\hat{\mathbf{y}}$; see inset). The resistance $R_{35,26}$ changes from a positive MR to negative as $\phi' \to 0°$. In both configurations, the negative MR appears only when **B** is aligned with **E**. (**C**) Conductance $G \equiv 1/R_{35,26}$. In weak B, it has the B^2 form predicted in Eq. 2 (*9*). A fit to the parabolic form gives $\tau_a/\tau_0 = 40$ to 60. (**D**) ρ_{xx} [as in (A)] extended to 35 T. Above 23 T, a knee-like kink appears at H_k. Above H_k, ρ_{xx} increases very steeply (for $\phi > 35°$).

As shown in Fig. 1D, the resistivity ρ_{xx} displays a large negative LMR (**B**$||\hat{\mathbf{x}}||$**I**, the current; the notch at $B = 0$ is discussed below). The resistance measured is $R_{14,23}$ (see Fig. 1C, inset). Raising T above ~100 K suppresses the peak. In Fig. 2C, ρ_{xx} (in samples J1 and J4) falls rapidly to saturate to an almost B-independent value above 5 T (the slight upturn is a hint that the axial current is sensitive to misalignment of **B** at the level ±1°). A large negative LMR is anomalous in a conventional conductor, even with band anisotropy (*18*).

The axial current is predicted to be large when **B** is aligned with **E**. A crucial test then is the demonstration that, if **E** is rotated by 90°, the negative MR pattern rotates accordingly; that is, the axial current maximum is locked to **B** and **E** rather than being pinned to the crystal axes, even for weak **B**.

To carry out this test, we rotated **B** in the x-y plane while still monitoring the resistance $R_{14,23}$. Figure 3A shows the curves of the resistivity ρ_{xx} versus B measured at 4.5 K at selected values of ϕ (the angle between **B** and $\hat{\mathbf{x}}$). The MR is positive for $\phi = 90°$ (**B**$||\hat{\mathbf{y}}$), displaying the nominal B-linear form observed in Cd_3As_2 (*20*) and Na_3Bi (*27*) with **B**$||$**c**. As **B** is rotated toward $\hat{\mathbf{x}}$ (ϕ decreased), the MR curves are pulled toward negative values. At alignment ($\phi = 0$), the longitudinal MR is very large and fully negative [see (*18*) for the unsymmetrized curves and results from sample J1].

We then repeated the experiment in situ with I applied to contacts 3 and 5, so that **E** is rotated by 90° (the measured resistance is $R_{35,26}$). Remarkably, the observed MR pattern is also rotated by 90°, even when $B < 1$ T. Defining the angle of **B** relative to $\hat{\mathbf{y}}$ as ϕ', we now find that the MR is fully negative when $\phi' = 0$. The curves in Fig. 3, A and B, are nominally similar, except that $\phi = 0$ and $\phi' = 0$ refer to $\hat{\mathbf{x}}$ and $\hat{\mathbf{y}}$, respectively. As we discuss below, we identify the locking of the negative MR direction to the common direction of **E**$||$**B** as a signature of the chiral anomaly.

The acute sensitivity of the axial current to misalignment at large B, as hinted in Fig. 2C, is surprising. To determine the angular variation, we performed measurements in which $R_{14,23}$ is measured continuously in fixed field versus tilt angle (with **B** either in the x-y or the x-z plane). Figure 4 displays the curves of $\Delta\sigma_{xx}(B, \phi) = \sigma_{xx}(B, \phi) - \sigma_{xx}(B, 90°)$ versus ϕ (**B** in the x-y plane at angle ϕ to $\hat{\mathbf{x}}$), with B fixed at values $0.5 \to 2$ T (Fig. 4A) and $3 \to 7$ T (Fig. 4B). Shown in Fig. 4, C and D, are the same measurements but now with **B** in the x-z plane at an angle θ to $\hat{\mathbf{x}}$. In both cases, the low-field curves ($B \leq 2$ T) are reasonably described with $\cos^p \phi$ (or $\cos^p \theta$) with $p = 4$. However, for $B > 2$ T, the angular widths narrow considerably. Hence, at large B, the axial current is observed as a strongly collimated beam in the direction selected by **B** and **E** as ϕ or θ is varied. The strong collimation has not been predicted.

The large negative MR in Fig. 3 implies a long relaxation time τ_a for the axial current. By fitting Eq. 2 to the parabolic profile of $G = 1/R_{35,26}$ shown in Fig. 3C, we find that $\tau_a = 40$ to $60 \times \tau_0$, the Drude lifetime. Despite its importance, the matrix element M in $1/\tau_a$ is not well studied. There is debate on whether a large node separation $2\delta k_N$ is needed to obtain a long τ_a [using the estimate (*18*) of $g^* \sim 20$, we find that $\delta k_N > k_F$ when

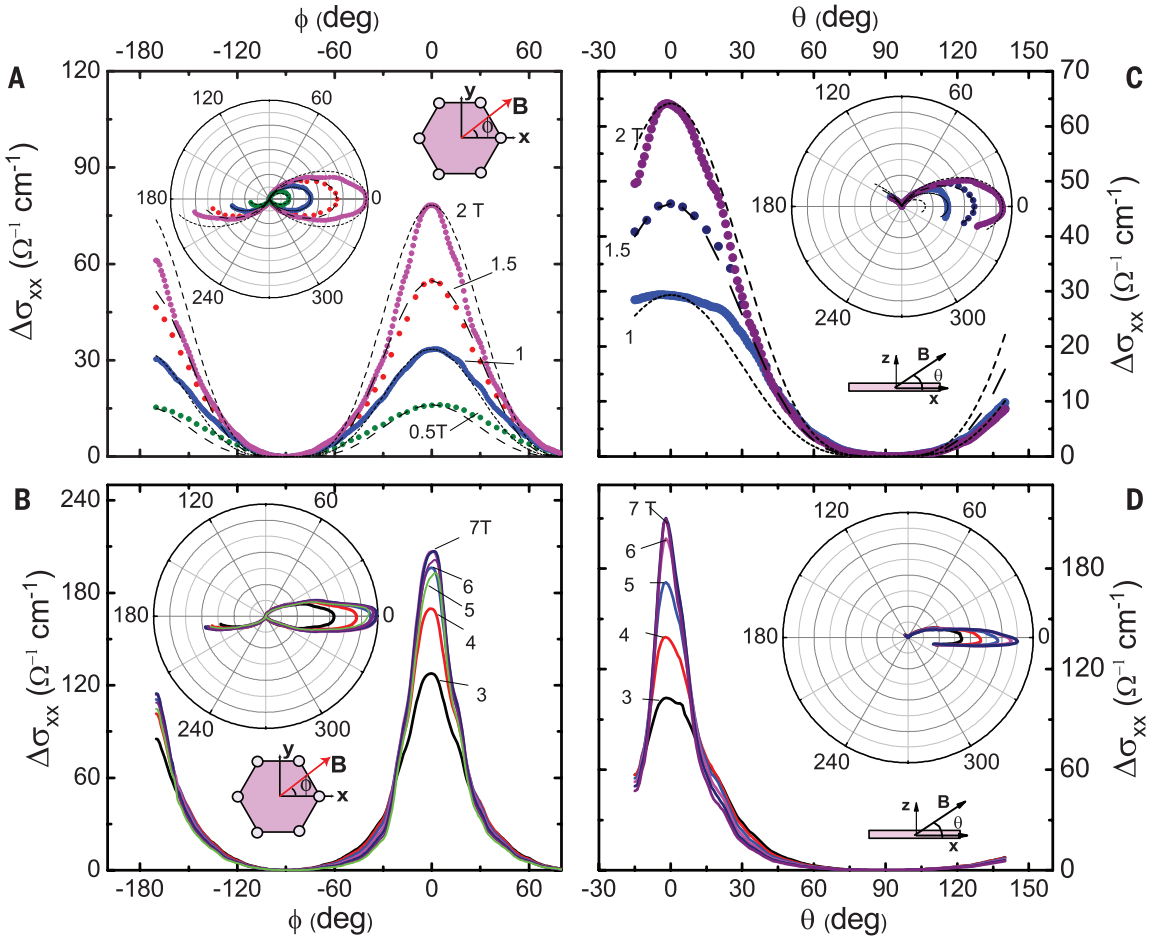

Fig. 4. Angular dependence of the axial current. The dependence is inferred from measurements of $R_{14,23}$ in tilted $\mathbf{B}(\theta,\phi)$ in sample J4 at 4.5 K. (**A** and **B**) **B** lies in the *x*-*y* plane at an angle ϕ to $\hat{\mathbf{x}}$ (sketch in insets). The conductance enhancement $\Delta\sigma_{xx}$ at fixed **B** is plotted against ϕ for values of $B \leq 2$ T (A) and for $3 \leq B \leq 7$ T (B). Fits to $\cos^4\phi$ (dashed curves), although reasonable below 2 T, become very poor as *B* exceeds 2 T. The insets show the polar representation of $\Delta\sigma_{xx}$ versus ϕ. (**C** and **D**) **B** is tilted in the *x*-*z* plane. As sketched in the insets, θ is the angle between **B** and $\hat{\mathbf{x}}$. Curves of $\Delta\sigma_{xx}$ versus θ for $B = 1$, 1.5, and 2 T are shown in (C); shown in (D) are curves for $3 \leq B \leq 7$ T. The axial current is peaked when $\phi \to 0$ (or $\theta \to 0$) with an angular width that narrows as *B* increases.

$B > 12$ T]. Recently, however, it was shown (*29*) that the ratio τ_a/τ_0 can be very large (in a superlattice model) even for negligible δk_N because Berry curvature effects hinder axial current relaxation and chiral symmetry is only weakly violated. This issue should be resolvable by LMR experiments.

A notable feature in the LMR profile (Fig. 1D) is the notch at $B = 0$, which persists to 120 K. Above 140 K, the notch expands to a V-shaped positive LMR profile. The insensitivity of this feature to the tilt angle of **B** implies that it is associated with the Zeeman energy. A similar feature is seen in Cd_3As_2 (*20*).

We extended measurements of $R_{14,23}$ to $B = 35$ T. From the curves of ρ_{xx} versus *B* (Fig. 3D), we find a new feature at the kink field $H_k \sim 23$ T when $\mathbf{B}||\hat{\mathbf{y}}$. As **B** is tilted away from $\hat{\mathbf{y}}$ ($\phi \to 55°$), the feature at H_k becomes better resolved as a kink. The steep increase in ρ_{xx} above H_k suggests an electronic transition that opens a gap. However, as we decrease ϕ below 45°, $H_k(\phi)$ moves rapidly to above 35 T. The negative MR curve at $\phi = 0$ remains unaffected by the instability up to 35 T (the small rising background is from a weak B_z due to a slight misalignment).

Within standard MR theory, the feature that is most surprising is the locking of the MR pattern to the **B** vector in Fig. 3, A and B. If one postulates that the narrow plume in Fig. 4 arises from anisotropies in the FS properties (v and τ_0 versus $\mathbf{k}$), the direction of maximum conductivity should be anchored to the crystal axes. We should not be able to rotate the resistivity tensor by orienting the weak *E* and *B* fields (this violates linear response). However, it agrees with the prediction of the chiral anomaly; the axial current peaks when **E** aligns with **B**, even for weak fields.

We believe that this locking pattern in weak *B* is the quintessential signature of the axial current. The experiment confirms the B^2 behavior in weak *B* and provides a measurement of τ_a. The narrow angular width of the axial current may provide further insight into its properties.

REFERENCES AND NOTES

1. E. M. Peskin, D. V. Schroeder, *Introduction to Quantum Field Theory* (Westview, Boulder, CO, 1995), chap. 19.
2. S. L. Adler, *Phys. Rev.* **177**, 2426–2438 (1969).
3. J. S. Bell, R. Jackiw, *Nuovo Cim.* **60A**, 4 (1969).
4. H. B. Nielsen, M. Ninomiya, *Phys. Lett. B* **130**, 389–396 (1983).
5. X. G. Wan, A. M. Turner, A. Vishwanath, S. Y. Savrasov, *Phys. Rev. B* **83**, 205101 (2011).
6. A. A. Burkov, M. D. Hook, L. Balents, *Phys. Rev. B* **84**, 235126 (2011).
7. K.-Y. Yang, Y.-M. Lu, Y. Ran, *Phys. Rev. B* **84**, 075129 (2011).
8. V. Aji, *Phys. Rev. B* **85**, 241101 (2012).
9. D. T. Son, B. Z. Spivak, *Phys. Rev. B* **88**, 104412 (2013).
10. S. A. Parameswaran, T. Grover, D. A. Abanin, D. A. Pesin, A. Vishwanath, *Phys. Rev. X* **4**, 031035 (2014).
11. P. Hosur, X. Qi, *C. R. Phys.* **14**, 857–870 (2013).
12. S. M. Young *et al.*, *Phys. Rev. Lett.* **108**, 140405 (2012).
13. C. Fang, M. J. Gilbert, X. Dai, B. A. Bernevig, *Phys. Rev. Lett.* **108**, 266802 (2012).
14. Z. J. Wang *et al.*, *Phys. Rev. B* **85**, 195320 (2012).
15. B.-J. Yang, N. Nagaosa, *Nat. Commun.* **5**, 4898 (2014).
16. Z. K. Liu *et al.*, *Science* **343**, 864–867 (2014).
17. S.-Y. Xu *et al.*, *Science* **347**, 294–298 (2015).
18. See supplementary materials on *Science* Online.
19. H.-J. Kim *et al.*, *Phys. Rev. Lett.* **111**, 246603 (2013).
20. T. Liang *et al.*, *Nat. Mater.* **14**, 280–284 (2015).
21. C. Zhang *et al.*, http://arxiv.org/abs/1504.07698 (2015).
22. Q. Li *et al.*, http://arxiv.org/abs/1412.6543 (2014).
23. C. Zhang *et al.*, http://arxiv.org/abs/1503.02630 (2015).
24. I. M. Tsidilkovskii, W. Giriat, G. I. Kharus, E. A. Neifeld, *Phys. Status Solidi B* **64**, 717–727 (1974).
25. N. Kikugawa *et al.*, http://arxiv.org/abs/1412.5168 (2014).
26. S. K. Kushwaha *et al.*, *APL Materials* **3**, 041504 (2015).
27. J. Xiong *et al.*, http://arxiv.org/abs/1502.06266 (2015).
28. S. Jeon *et al.*, *Nat. Mater.* **13**, 851–856 (2014).
29. A. A. Burkov, *Phys. Rev. B* **91**, 245157 (2015).

ACKNOWLEDGMENTS

We thank B.A. Bernevig and Z. Wang for valuable discussions. Supported by Army Research Office grant ARO W911NF-11-1-0379, a MURI award for topological insulators (ARO W911NF-12-1-0461), and the Gordon and Betty Moore Foundation's EPiQS Initiative through grant GBMF4539 (N.P.O.). The growth and characterization of crystals were performed by S.K.K., J.W.K., and R.J.C. with support from NSF grant DMR 1420541. Some experiments were performed at the National High Magnetic Field Laboratory (NHMFL), which is supported by NSF Cooperative Agreement no. DMR-1157490, the State of Florida, and the U.S. Department of Energy; we thank E. S. Choi for assistance at NHMFL.

SUPPLEMENTARY MATERIALS

www.sciencemag.org/content/350/6259/413/suppl/DC1
Materials and Methods
Supplementary Text
Figs. S1 to S6
References (*30*, *31*)

3 February 2015; accepted 19 August 2015
Published online 3 September 2015
10.1126/science.aac6089

Evidence for the chiral anomaly in the Dirac semimetal Na_3Bi

Jun Xiong, Satya K. Kushwaha, Tian Liang, Jason W. Krizan, Max Hirschberger, Wudi Wang, R. J. Cava and N. P. Ong

Science **350** (6259), 413-416.
DOI: 10.1126/science.aac6089originally published online September 3, 2015

Breaking chiral symmetry in a solid

Dirac semimetals have graphene-like electronic structure, albeit in three rather than two dimensions. In a magnetic field, their Dirac cones split into two halves, one supporting left-handed and the other right-handed fermions. If an electric field is applied parallel to the magnetic field, this "chiral" symmetry may break: a phenomenon called the chiral anomaly. Xiong *et al.* observed this anomaly in the Dirac semimetal Na_3Bi (see the Perspective by Burkov). Transport measurements lead to the detection of the predicted large negative magnetoresistance, which appeared only when the two fields were nearly parallel to each other.

Science, this issue p. 413, see also p. 378